Nanoscale

Accepted Manuscript

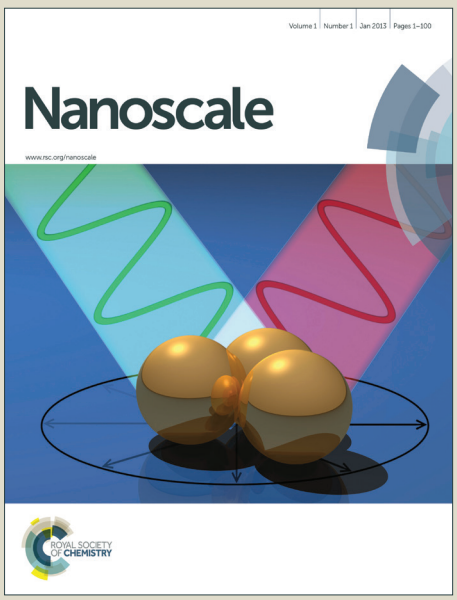

ROYAL SOCIETY OF CHEMISTRY

www.rsc.org/nanoscale

Green and scalable production of colloidal perovskite nanocrystals and transparent sols by a controlled self-collection process

Shuangyi Liu[1,2,3,4], Limin Huang[5,1,*] Wanlu Li[1,2,6], Xiaohua Liu[1,2,6], Jing Shui[5], Jackie Li[3], and Stephen O'Brien[1,2,3,6*]

[1]The CUNY Energy Institute, City University of New York, Steinman Hall, 160 Convent Avenue, The City College of New York, New York, NY 10031, USA.

[2]Department of Chemistry, The City College of New York, Marshak Building, 160 Convent Avenue, NY 10031, USA

[3]Department of Mechanical Engineering, The Grove School of Engineering, Steinman Hall, 160 Convent Avenue, The City College of New York, New York, NY 10031, USA

[4]Chongqing Institute of Green and Intelligent Technology, Chinese Academy of Sciences, Chongqing 400714, P. R. China.

[5]Department of Chemistry, South University of Science and Technology of China, Shenzhen 518055, P. R. China

[6]The Graduate Center of the City University of New York, 365 Fifth Avenue, New York, NY 10016 USA.

*Corresponding authors: sobrien@ccny.cuny.edu and huanglm@sustc.edu.cn

Abstract:

Colloidal perovskite oxide nanocrystals have attracted a great deal of interest owing to the ability to tune physical properties by virtue of the nanoscale, and generate thin film structures under mild chemical conditions, relying on self-assembly or heterogeneous mixing. This is particularly true for ferroelectric/dielectric perovskite oxide materials, for which device applications cover piezoelectrics, MEMs, memory, gate dielectrics and energy storage. The synthesis of complex oxide nanocrystals, however, continues to present issues pertaining to quality, yield, % crystallinity, purity and may also suffer from tedious separation and purification processes, which are disadvantageous to scaling production. We report a simple, green and scalable "self-collection" growth method that produces uniform and aggregate-free colloidal perovskite oxide nanocrystals including $BaTiO_3$ (BT), $Ba_xSr_{1-x}TiO_3$ (BST) and quaternary oxide $BaSrTiHfO_3$ (BSTH) in high crystallinity and high purity. The synthesis approach is solution processed, based on the sol-gel transformation of metal alkoxides in alcohol solvents with controlled or stoichiometric amounts of water and in the stark absence of surfactants and stabilizers, providing pure colloidal nanocrystals in a remarkably low temperature range (15 ˚C -55 ˚C). Under a static condition, the nanoscale hydrolysis of the metal alkoxides accomplishes a complete transformation to fully crystallized single domain perovskite nanocrystals with a passivated

surface layer of hydroxyl/alkyl groups, such that the as-synthesized nanocrystals can exist in the form of super-stable and transparent sol, or self-accumulate to form a highly crystalline solid gel monolith of nearly 100% yield for easy separation/purification. The process produces high purity ligand-free nanocrystals excellent dispersibility in polar solvents, with no impurity remaining in the mother solution other than trace alcohol byproducts (such as isopropanol). The afforded stable and transparent suspension/solution can be treated as inks, suitable for printing or spin/spray coating, demonstrating great capabilities of this process for fabrication of high performance dielectric thin films. The simple "self-collection" strategy can be described as green and scalable due to the simplified procedure from synthesis to separation/purification, minimum waste generation, and near room temperature crystallization of nanocrystal products with tunable sizes in extremely high yield and high purity.

Introduction

Perovskite complex oxides exhibit a wide range of unique chemical and physical properties associated with the formula ABO_3 structure, which is available for a variety of ionic composition, doping and substitution. Barium titanate ($BaTiO_3$, or BT) and its various doped or substituted derivatives are the most valuable and most investigated perovskite materials for multilayered capacitors (or MLCC), non-volatile memory, uncooled IR detectors, positive temperature coefficient of resistivity (PTCR) thermistors, multiferroics, energy storage and conversion, due to the high dielectric performance, attractive ferroelectric, pyroelectric, piezoelectric, electrooptic and catalytic properties [1]. Other barium-based perovskite complex oxides have also received much attention due to their potential applications in tunable nonlinear optics and oxygen evolution catalysts for solar energy conversion [2].

With the continuous trend toward miniaturization and complexity in integrated electronics, highly crystalline monodisperse and aggregate-free perovskite oxide nanocrystals, can be viewed as "building blocks" for assembly through various low temperature solution processing methods, such as ink-jet printing, spraying or spin-coating.[3] They are highly desirable not only for studies of size dependent properties, but also for manipulation, thin film processing and incorporation of the nanocrystals into various electric, electronic, optical, mechanical and biomedical devices, including the possibility of self-assembly into nanocrystal superlattices for new applications. Aggregate-free nanocrystals are critical to make stable and transparent pure nanocrystal or nanocomposite solutions for field-responsive "smart fluids"[4], improvement of dielectric response of liquid crystal to electric field[5], and they also have promising biomedical applications such as in-vivo imaging and cellular nanovectors for drug delivery [6]. The stable solution is printable and especially highly desirable for making crack-free thin films on flexible substrates that can be used in high k gate dielectrics for organic electronics (such as OLED, OTFT), energy storage [7], and energy conversion (such as flexible nano-generators)[1j, 8]. The nanocrystal thin films also provide a convenient way to process densified thin films by low temperature sintering or laser pulse sintering [1a, 9].

Solution processing routes to colloidal nanocrystals are advantageous among a wide variety of synthetic approaches in terms of control from molecular precursors to the final aggregate-free products under moderate conditions (T< 300 ˚C). Many current techniques for the solution phase synthesis of uniform $BaTiO_3$ based nanocrystals require either stringent solvothermal/hydrothermal conditions or extreme pH (pH>13) in the presence of organic ligands or surfactants[2c, 10]. And, a great deal of effort is needed for nanocrystal collection, yield and purification. For instance, the isolation of aggregate-free nanocrystals with semi-uniform size may require multiple dispersion-centrifugation cycles, which consumes a large quantity of solvent. The presence of barium carbonate, $BaCO_3$, up to wt % of 5-10, is a common problem. Few synthesis processes can be viewed as readily scalable for mass production. Recently, a sol-gel process involving a kinetic diffusion of water/HCl vapor at the gas-liquid interface of a bimetallic alkoxide precursor was reported to produce high purity BT nanocrystals near room temperature, and the kinetically controlled diffusion process was proven to be scalable to 250 g of $BaTiO_3$ nanoparticles in a single batch. Although, the complexity of apparatus required and choice of chemicals may limit the feasibility of large scale production[11].

Here we report a simple, green and scalable self-collection growth technology that produces size-tunable highly pure and crystalline colloidal ligand-free $BaTiO_3$-based nanocrystals in the low temperature range between 15 ˚C and 55 ˚C under static conditions. With the control of concentrations of water and metal oxides, the hydrolysis of metal alkoxides in ethanol solvent is carefully tuned to trigger the “self-collection” of high purity colloidal nanocrystals. In a simple container all the sources can be converted and self-accumulated to form a pure and highly crystalline gel monolith solid product that is well separated from a liquid phase (hence “self-collection” process). The only byproduct is alcohol such as isopropanol. The nanocrystal product can be readily collected and purified without centrifugation or filtration, achieving nearly 100% yield, while the liquid phase is recyclable because it contains ethanol solvent as majority and trace amount of the byproduct such as isopropanol, with negligible waste generation. In addition, the uniform BT-based nanocrystals can also be obtained at a temperature as low as 15 ˚C while maintaining high quality in terms of crystallinity, purity, size uniformity and dispersibility. The self-collection synthesis technique is advantageous for scale-up production because it forms under static conditions, does not require complex apparatus, and the product crystal size is only sensitive to water content.

We offer our procedure as a potentially ideal means to produce perovskite nanocrystals as components for low temperature processing of nanocomposites (2-2 or 3-0 polymer-particle nanocomposites) in the dielectric layer of solid state parallel plate capacitors. The challenge faced by researchers in this field is not simply to attain a high value permittivity of a film, since this by itself is not an indication of device functionality or capability. Instead, the comprehensive dielectric performance must be assessed, in which loss (referred to as dissipation factor, or tan δ, unit less) and voltage tolerance (similar to dielectric strength or breakdown strength, with units kV/mm or MV/m) play a pivotal role. An important first step is to show the frequency dependent

behavior of the effective permittivity with concurrent low loss over a wide frequency range. A flat or gently sloping line is strong indication of dielectric performance due to the intrinsic behavior of the material, as opposed to contributions from adsorbates, water, free ions or other space charge effects which increase the value of permittivity at low frequency impedance and plague the materials chemistry literature. It is only natural, after all, that solution-processed methods would lead to such results. However, the field needs to move towards producing nanocomposite films whose performance is not confused with contributions from extrinsic effects that offer no technological advancement. Achieving a stable and low loss ultimately translates to a low ESR value, and is a critical advancement. Low loss is an indication of suppression of space charge effects, and defects in the dielectric layer. In addition, low loss offers promise that the voltage tolerance will be higher, since the percolation threshold of the nanocomposite layer - the ability for the dielectric to remain insulting and not let current pass through it – depends upon eliminating stray charges, ions, and defects, improving passivating layers of the nanoparticles, improving the interface between polymer and nanoparticle, reducing void space within the composite, and producing a more densely compact, more functional film.

Experimental

Synthesis: The synthesis of barium titanate-based nanocrystals is based on the treatment of a metal-organic source in ethanol/H_2O solvent (water: 2.0-5 vol%). For a typical synthesis of barium strontium titanate nanocrystals (BST, $Ba_{0.7}Sr_{0.3}TiO_3$ as an example), 1.238 g barium isopropoxide ($Ba(OiPr)_2$, iPr = $CH(CH_3)_2$, Alfa Aesar, 99.9%) and 0.417g strontium isopropoxide ($Sr(OiPr)_2$, Aldrich, 99.9%) were first dissolved in 80 ml 200 proof ethanol, then 2 ml titanium isopropoxide ($Ti(OiPr)_4$, Alfa Aesar, 97%) was added under stirring to form a transparent solution. After stirring for 5 min, 20 ml ethanol (contain water ~10 vol%) was added slowly under stirring to form a clear and transparent solution (concentration of metal organic source: ~ 0.068 M). The stirring process was kept for 10-20 mins until the solution gradually turned into a viscous clear gel. Dissolving metal organic sources in alcohol was conducted in a N_2-protected box to avoid initial exposure of the sources to oxygen and water. Once the clear solution was formed, the stirring bar was removed, and the solution was sealed in a closed container. The container with the solution was transferred out of the box and kept under ambient conditions. After the clear gel was kept still at just below room temperature (15 ˚C in the present case) for 4-10 hrs (so-called aging process), it was warmed in an oven with a temperature of 45-55 ˚C for 2-10 hrs to form a self-accumulated solid gel monolith product. The gel product can also be formed at a lower temperature (15 ˚C) under static conditions. The monolith solid product was collected from the solution, and rinsed with ethanol. The product could be then sonicated with calculated amount of solvents, such as ethanol or furfural alcohol, to afford a transparent nanocrystal solution with a concentration of 10-50 mg/ml. For the synthesis of four-cation perovskite nanocrystals, hafnium (IV) n-butoxide was used as a Hf source to synthesize $Ba_{0.65}Sr_{0.35}Ti_{0.5}Hf_{0.5}O_3$ (BSTH) as an example. Compared to $Ba(OiPr)_2$ source, less expensive Ba metal (0.5% strontium) can also be used as a Ba source. In a typical synthesis, 0.719 g Ba metal

was first dissolved in 32 ml of anhydrous ethanol under dry N_2 protection to form a clear solution. After adding 1.5 ml of $Ti(OiPr)_4$ and 32 ml ethanol (contain water ~10 vol%), a gradual gelation can be observed at room temperature. After aging at room temperature for 3 days, the immobile clear gel turned into a white and semi-transparent gel monolith at an elevated temperature (55 ˚C) within hours.

Characterization: The X-ray powder diffraction (XRD) patterns were collected in the 20−70° 2θ range using a PANalytic PW 3040/60 X-ray diffractometer using a Cu Kα radiation (λ = 1.5406 Å). Transmission Electron Microscopy (TEM) was performed on a JEOL 100CX microscope and JEM-2100 LaB6 microscope. Specimens for TEM were prepared by placing a drop of dilute nanocrystal solution in ethanol on a carbon coated copper grid (Ted Pella, Inc.). The particle size statistics (size average and standard deviation) were calculated using Excel statistical tool based on the size measurement of 200-300 nanocrystals for each sample using a size analyzing software Nano Measure1.2. Scanning Electron Microscopy (SEM) was performed on a Zeiss Supra55VP field emission SEM. Thin films were cross-sectioned by cleaving and analysis. Raman spectra were recorded in the 100-1000 cm^{-1} wavenumber range using a Horiba Jobin Yvon Model HR800 Raman microscope at room temperature. Dry powder samples were placed on glass slides and excited with 632.8 nm HeNe laser radiation. Multiple spin coatings can be applied to achieve layer structures in the range of nanometer to micrometer thickness. Frequency dependence of the capacitance, dielectric loss and equivalent series resistance (ESR) were measured using an Agilent 4294A Precision Impedance Analyzer. The comprehensive dielectric performance measurement was described previously.

Results

In the case of barium strontium titanate, a variety of stoichiometries are possible (x = 0.1, 0.2 etc.). One of our preferred stoichiometries for it's dielectric response is $Ba_{0.7}Sr_{0.3}TiO_3$. $Ba_{0.7}Sr_{0.3}TiO_3$ is used as an example to further illustrate the synthesis procedure, to discuss the reaction process, the mechanism, and the structure. We refer to barium strontium titanate as BST throughout this report. For BST synthesis, a clear and transparent solution was first prepared by simply dissolving Ba, Sr and Ti metal alkoxides in ethanol solvent to achieve a concentration of metal organic sources around 0.07 M. After further addition of controlled amounts of ethanol/water under stirring, the solution gradually turned into more clear and transparent, and thickened. The solution was then transferred to any closed plastic or glass container for gelation, aging and crystallization. The formation of ABO_3 nanocrystals was initiated by slightly warming the immobile clear gel at a temperature between room temperature and 55 ˚C. The higher the temperature, the faster the product starts to crystallize. In Figure 1a, a semitransparent white solid gel as well as a clear liquid phase starts to appear after warming the solid clear gel at 55 ˚C for 2 hrs. The white gel gradually shrinks into a denser gel rod (or monolith) accompanied with the formation of more transparent liquid phase over a time period of 2-6 hrs, and the solid product does not change in appearance after 5 hrs. The obvious advantage of the synthesis is that under static conditions the solid product can be self-accumulated to a gel monolith (what we

refer to as self-collection) that facilitates the collection/separation of the product from liquid phase and the subsequent solvent rinsing. Powder XRD profiles (Figure 1b) and EDX spectrum (Supplementary Fig. S1) show that the self-collected products synthesized at various temperatures and crystallization times (2-5 hrs) are pure BST crystal phases with no observable traces of $BaCO_3$ and TiO_2 impurities. The broad diffraction peaks suggest the products are in the nanometer size range, and the size can be estimated to be ~6.6 nm for the sample crystallized at 55 ^oC for 5 hrs according to the peak (110) broadening based on Debye Scherer equation (line broadening due to instrument itself not corrected) (Supplementary Table S1). However, as expected, the diffraction peaks are too broad to sufficiently distinguish between cubic and tetragonal polymorphs. In addition, Raman spectroscopy also confirms a pseudocubic structure at room temperature with weak local tetragonal distortion arising from the off-centering of titanium atoms (Supplementary Fig. S2). Furthermore, it was found that the self-collected gel product can be obtained even at a lower temperature (15 ˚C) after a longer crystallization time (days vs hrs). A semitransparent gel-like solid product started to appear in 7 days, which gradually turned into a denser gel monolith within 4 weeks (15 ˚C) (Supplementary Fig. S3). The solid products at different time intervals were also verified to be pure BST nanocrystals by XRD and EDX.

Likewise, the self-collection strategy can be extended to the synthesis of perovskite complex oxide nanocrystals $(Ba_xSr_{1-x})(Ti_yHf_{1-y})O_3$, with the composition of $Ba_{0.65}Sr_{0.35}Ti_{0.5}Hf_{0.5}O_3$ (BSTH) as an example. The crystal structure and composition of BSTH was confirmed by XRD (Fig. 1d) and EDX (Supplementary Fig. S4). The XRD patterns (Figure 1d) show that the diffraction peaks shift to higher 2Theta with the substitution of Ba cations (r_{Ba2+} ≈149 pm) with smaller Sr cations (r_{Sr2+} ≈132 pm) due to a lattice contraction with substitution of the A sites of ABO_3 perovskite structure (black pattern vs. red pattern), while the diffraction peaks shift to lower angles with the substitution of Ti cations (r_{Ti4+} ≈ 61 pm) with larger Hf cations (r_{Hf4+}≈ 85 pm) due to a lattice expansion with substitution of the B sites of ABO_3 perovskite structure (red pattern vs. blue pattern) (Supplementary Table S2). Furthermore, for the BSTH structure, the significant decrease in the intensity of the diffraction peaks corresponding to the (100), (111), and (210) planes can be observed (Figure 1d, blue pattern). By considering the structure factors F_{hkl}, such as $F_{100} = F_{210} = f_A - f_B - f_O$ and $F_{111} = f_A - f_B + 3f_O$, where f_A, f_B, and f_O are the atomic scattering factors of A and B site cations and oxygen of the ABO_3 structure, respectively[2a], the intensity decrease could be explained as follows. The substitution of Ti cations with Hf cations results in the increase of f_B, which in turn reduces the intensity of the corresponding diffraction peaks, such as F_{100}, F_{111}, and F_{210}. The XRD results indicate the exclusive presence of perovskite phase of various compositions (BT, BST, and BSHT) in high crystallinity and high purity.

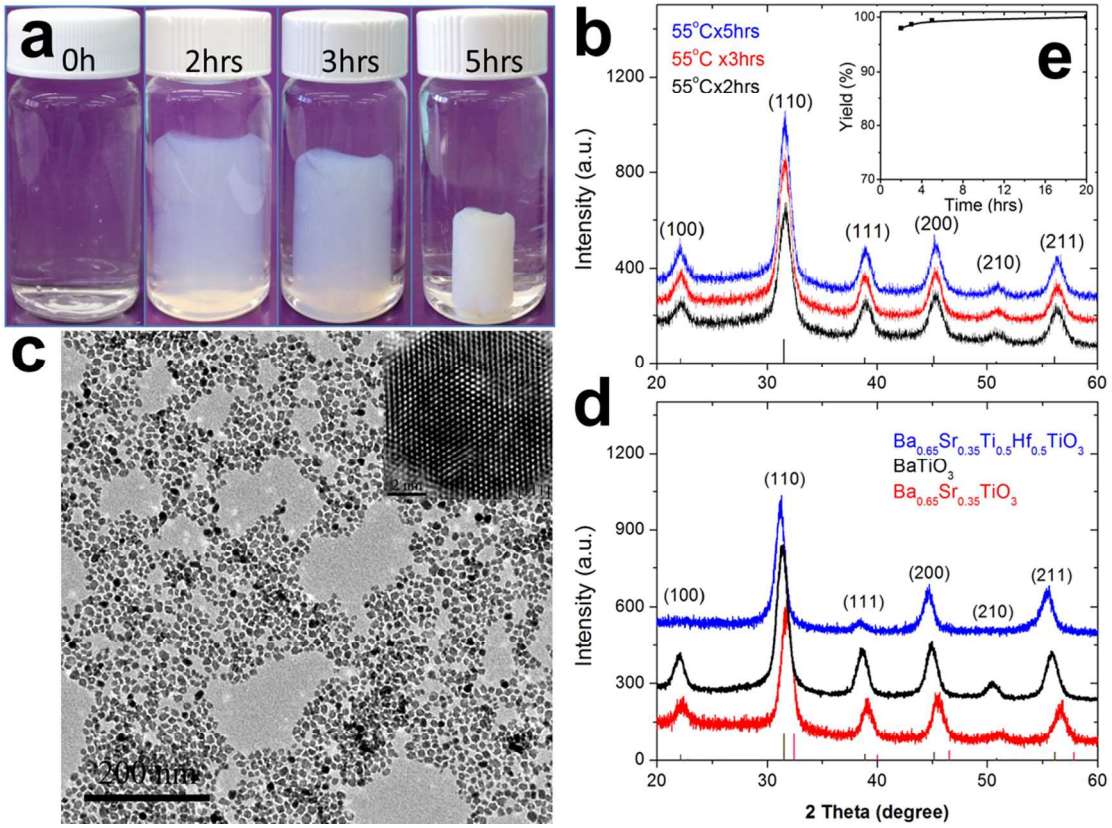

Figure 1.

(a) Photo images, (b) XRD patterns and yields (inset) of BST nanocrystals evolution with the crystallization time at 55°C, respectively. (c) TEM image of BST nanocrystals (inset: high-resolution image of a particle oriented along the [111] direction). (d) XRD of various BT-based perovskite nanocrystals. The stick patterns for $BaTiO_3$ (ICSD #029147, in black) and $SrTiO_3$ (ICSD# 080874, in red) are included in (b) and (d).

While color of precursors can be somewhat arbitrarily dependent on source or vendor, color and color change is a useful guide for in the lab. We wish to include our own experience for the benefit of researchers exploring these procedures: when using brown or orange colored sources of $Ba(OiPr)_2$ or $Sr(OiPr)_2$ as a metal-organic source (Aldrich or Alfa Aesar, as purchased), the product self-accumulated to form a dense yellow gel monolith over the time, while the originally yellow colored mother solution became almost colorless with the formation of the gel monolith (Supplementary Figure S5). This suggests that the liquid phase contain few metal organic sources, and almost all the colored sources can be transferred to the final crystallized solid product, which is a BST phase in high purity and high crystallinity. ^{1}H NMR analysis of the mother solution after reaction shows that the liquid phase is composed of ethanol solvent as significant majority and trace amount of isopropanol from the hydrolysis/condensation of metal isopropoxides (Supplementary Figure S6a), and a preliminary study also proves that the liquid phase contains no metal organic residue, confirming the total conversion of metal organic sources to final products. Since the solid gel product can be easily collected by simply removing the liquid phase, rinsed and purified with little waste, the yield of the final solid product attained

is >95% in ~2 hrs and achieves almost 100% after 5 hrs (Figure 1b, inset). This method is contrary to most solution based synthesis of nanocrystal products, in which lengthy separation and purification is required, involving high speed centrifugation and centrifugation/dispersion cycles.

The solid gel monolith obtained can be described as a collection of loosely bound monodisperse nanocrystals. It is not composed of strongly bonded aggregates. The nanocrystals can be easily dispersed in many solvents (mainly polar, e.g. ethanol or furfural alcohol) under regular sonication. For instance, it took about 30 mins of sonication in a 50 Watt sonication bath until a highly transparent nanocrystal solution was obtained with adjustable concentration in different solvents (such as up to 50 and 80 mg/ml in ethanol and furfuryl alcohol respectively. It was found that the solution has long and stable shelf life (> 2.5 years so far) with no observable sediments although it contains no additional surfactants or stabilizers. When putting a drop of dilute nanocrystal solution (ethanol as solvent) on a Cu TEM grid, the TEM images show that nanocrystals are uniform in size and aggregate free (Figure 1c). Typically, the nanocrystals have tunable sizes in the range of 7-12 nm and uniform sizes with deviation less than 7% (s.d.< 7%) The crystal sizes depend almost entirely on the controlled water content (as opposed to temperature or processing time, see Figure 2), consistent with the XRD results. High-resolution TEM images of individual nanocrystals show that these particles are single crystals. The aggregate-free nature of the nanocrystals is advantageous in terms of forming stable and transparent nanocrystal suspensions, and the subsequent incorporation of the nanocrystals into various platforms that can ultimately lead to electronic, optical, mechanical and biomedical devices, is immediately apparent.

We found that the diameters of nanocrystals change little with the crystallization temperature (15 ˚C- 190 ˚C) or time (> 4 hrs), as clearly indicated in Figure 2a, and are only really sensitive to water content in the system. For example, the crystal sizes change little (~ 9-10 nm) no matter the crystallization temperatures (15-190 ˚C) when the water content is 5 vol% (all the crystal sizes are within error bar), but the sizes are tunable between 7 and 12 nm while altering the water content from 2.5 vol% up to 10 vol%. It suggests that the nanocrystals are produced via a LaMer model, in which the nucleation is a fast process followed by a slow crystal growth process without further nucleation.[12]

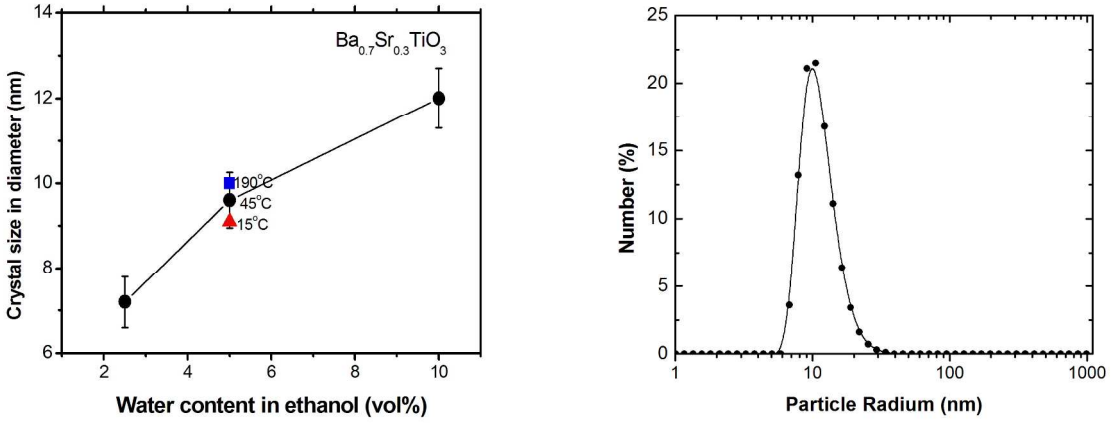

Figure 2. (a) Diameter of BST nanocrystals as a function of water content in ethanol solvent. The composition of BST precursor solution is $Ba(OiPr)_2$+$Sr(OiPr)_2$+$Ti(OiPr)_4$ + ethanol/H_2O. The crystal size range is the error bar nanocrystals synthesized at the temperature of 15 -190 ˚C(red triangle: 15 ˚C, black cycle: 45 ˚C, and blue cube: 190 ˚C). (b) Size distribution of BST nanocrystals by number (measured by dynamic light scattering).

The nanocrystal solution was characterized by dynamic light scattering (DLS) and electrophoretic light scattering (Figure 2b). The hydrodynamic sizes (in radium) and zeta potentials of the nanocrystals in ethanol were measured to be ~10 nm and ~+30 mV, respectively. The zeta-potential of ~+30 mV suggests the nanocrystal surface carry positive charges, which provide electrostatic repulsion among the nanocrystals to prevent them from clumping together even without the presence of surfactant. The peak at the particle size distribution (Figure 4) is higher than that from the TEM observation. DLS is known to return larger sizes for this nanoscale regime, given the nature of the instrumental measurement and theory in calculation. It may also suggest that the nanocrystals in solution exist as a dynamic form of twins or triplets, although the TEM image clearly shows the nanocrystals are individually aggregate-free when deposited. The result is consistent with previous reports on DLS measurement of stable BT nanocrystal suspensions.[7c, 7d] The DLS results also suggest that the nanocrystals in solution are stable, and most likely, the stability in ethanol arises from electrostatic repulsion among the positively charged nanocrystals. In order to analyze more closely the surface structure of the BST nanocrystals we performed Fourier transform infrared (FT-IR) spectroscopy, shown in Figure 3. The spectra show that on the nanocrystal surface there are a large number of hydroxyl groups (-OH, corresponding to a strong and broad absorbance peak in the range 3400-3500 cm^{-1}) as well as a trace number of hydrocarbon ending groups (-CH, 2900 cm^{-1}). The combination of –OH and -OR or –R groups (R = CH_3, CH_2CH_3, $CH(CH_3)_2$) gives rise to a polar surface favorable to dispersion in polar solvents, but one that is not completely hydrophilic. In fact the contribution of hydrophobicity from the alkyls belonging to the alkoxy surface groups are likely contributing

to the stabilization of the aggregate-free nanocrystals in polar organic solvents such as alcohols, and the organic ending groups may further provide surface barriers to prevent the nanocrystals from clumping together, where otherwise, in a scenario where there are a preponderance of –OH groups, non-reversible aggregation occurs more readily. The alkoxy groups on the surface of the nanocrystals could be viewed as mildly "protecting" for dispersion stabilization, while offering the possibility for further chemical modification.

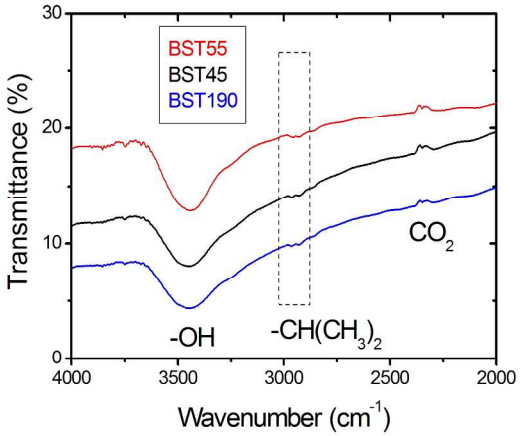

Figure 3. IR spectra of BST nanocrystals synthesized at different temperatures.

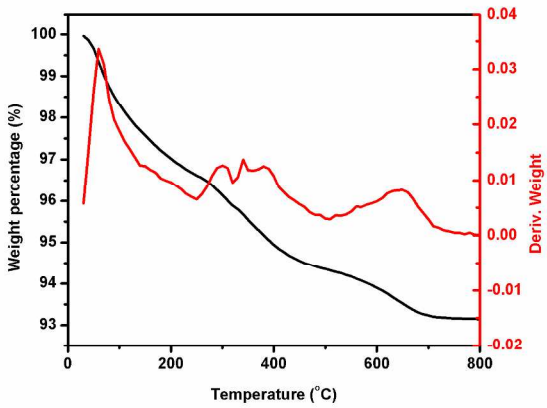

Figure 4. TG/DTG profile of air dried samples of BST nanocrystals.

To enable further characterization of the surface, we performed thermal analysis of the nanocrystals using thermo gravimetric/differential thermal analysis. TG/DTG analysis in flowing air was performed on air dried samples of the ~8 nm BST nanoparticles and the results are shown in Figure 4 (see also Supplementary information, Figure S2 for the profile recorded in $N_{2(g)}$). The DTG curve, the first peak reveals a 2.5 % weight loss around 60°C, due to the evaporation of volatile components, namely ethanol and possibly some residual water. The second weight loss (3%) at the temperatures between 304°C -386 °C is assigned to the combustion/carbonization of the organic derivatized surface alkoxy groups (-$OCH(CH_3)_2$, -OCH_2CH_3). The subsequent weight loss (wt 1%) at 650°C is can be ascribed to condensation of remaining hydroxyl groups on the surface of the nanocrystals (e.g. Ti-OH + TiOH -> Ti-O-Ti + H_2O) on the surface of the nanocrystals.

With respect to surface chemistry and dispersibility, we conclude that the individual nanocrystals are loosely interconnected in the monolith and have subsequent good dispersibility in organic polar solvents owing to an abundance of surface hydroxyl groups and some alkoxy/alkyl groups, that help contribute to a tendency towards loose and reversible aggregation. With the total absence of surfactants or stabilizers, they are highly dispersed in alcohol solvents such as ethanol

or furfuryl alcohol (FA) under gentle sonication to afford clear and stable solution with adjustable concentrations as high as 50 mg/ml (Figures 5a, 5b). In particular, BST nanocrystals/furfuryl alcohol (FA) mixture forms a transparent (brown) solution that can be stable for at least 2.5 years without sedimentation (Figure 5b), and the particle size distribution in the solution remains unchanged over this time according to the DLS measurement. The aggregate-free nanocrystal can also be easily incorporated into other media such as a variety of polymers, and the abundance of surface hydroxyl groups also open up a route to surface linkage with other functionalities without post-treatment with agents such as H_2O_2[13]. In addition, in some cases monomers were used initially and later converted to polymerized forms to better prepare nanocomposites, and strong interactions between nanocrystal and the polymer have been demonstrated[14]. For instance, nanocrystal/ polymer composite thin films were fabricated by spin-coating, printing or spraying a nanocrystal/furfuryl alcohol solution in which furfural alcohol is used as a solvent as well as a monomer for poly(furfuryl) alcohol (PFA)[14]. In Figure 5c, a uniform and dense BST/PFA nanocomposite thin film with high dielectric performance and good mechanical strength was prepared by printing a transparent BST nanocrystals/FA ink solution or spin (or spray) coating a BST/FA/EtOH ink solution (co-solvents FA and ethanol) followed by in-situ polymerization of FA upon heat treatment at 80 ˚C -100 ˚C (Figure 5c). Electrical measurement shows that the BST/PFA thin film has stable and high capacitance density (or high effective dielectric constant of above 20) and low dielectric loss (< 5%) in a wide frequency range of 100Hz and 1MHz under ambient conditions (Figure 5d). The slight uptick in dielectric loss is due to the contact resistance which is known to make a significant contribution to the dielectric loss is at higher frequencies. A further explanation of this phenomenon is provided in the supplementary information (Supplementary Figure S10). It is an extrinsic effect dependent upon choice of metal electrode (whether Al, Ag, Au, Cu etc.), quality (grain size, thickness, surface adhesion to the dielectric layer) of the metal electrodes, and the deposition process (sputtering, evaporation etc.). Contact resistance can be improved through further materials research on this topic, and finding electrodes that are more compatible to the dielectrics or higher quality electrodes preparation process[14].

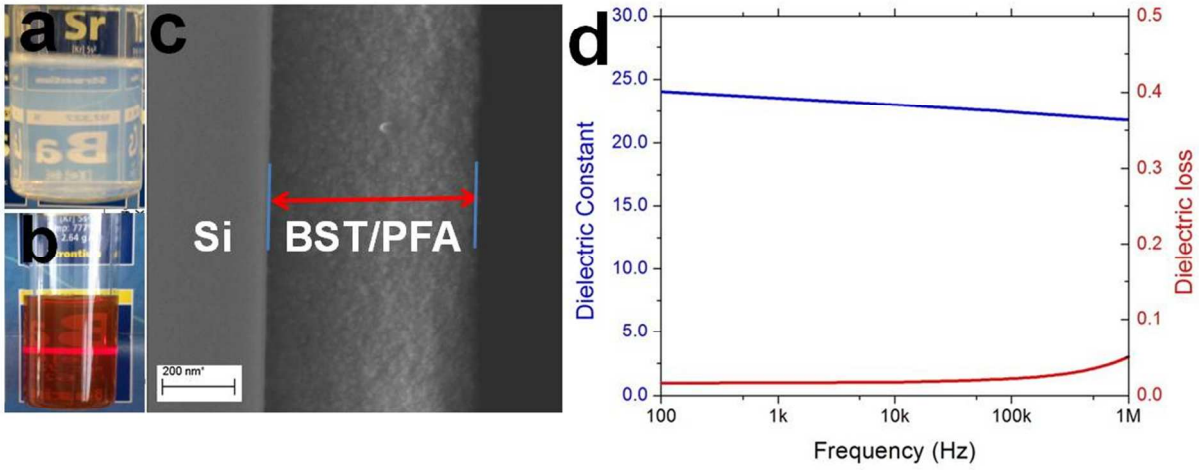

Figure 5. Printable BST nanocrystal solution (a) ethanol as solvent (40 mg/ml) and (b) FA as solvent (50 mg/ml), a red (633 nm) laser beam travelling through the transparent solution, showing the Tyndall effect and confirming a uniform colloidal dispersion of nanocrystals; (c) cross-section SEM image of a BST/PFA nanocomposite thin film, and (d) dielectric properties of a BST/PFA thin film.

Discussion

The present method distinguishes itself from traditional sol-gel methods by the additional features of the self-collection process we describe, and, notably, the low temperature nanoscale crystallization approach, realized through the addition of precisely controlled amounts water under nitrogen protected non-humid conditions. Scheme 1 summarizes the relationship between the concentrations of water and metal-organic species (MO) and gel formation at room temperature (T=15 ˚C). When there was no/less water in the ethanol solution of BST precursors (Scheme 1, zone I), there is no obvious and instant reaction being detected, as can be proven by ^{1}H NMR spectrum of ethanol solution of precursors (Supplementary Fig. S6b),only metal-organic precursors based white precipitate appeared within 2-3 hrs at room temperature instead of forming a transparent gel. The following crystallization of BST phases required much higher solvothermal temperature (as high as 200 ˚C) and longer time (>2 days) based on a pure alcoholysis process since it is a slower process than hydrolysis. On the other hand, when water content was higher than 15 vol%, the hydrolysis occurred so fast that a glue-like opaque suspension was formed other than a transparent solution/gel which could not be converted to a solid gel monolith (Scheme 1, zone II). Therefore, the water content in the system needs to be well controlled for the self-collection synthesis. A suitable amount of water in the system is found to be within 2-10 vol% (with approximate concentrations of 1.11-5.56 mM) (Scheme 1, zone III), and the hydrolysis of metal-organic sources (i.e. BST precursors) occurred slowly and

controllably (molar ratios of $[H_2O]/[MO]_{total}$ = 8-40) so that the solution initially stayed clear and transparent, and with the gradual hydrolysis and cross-linking it finally turned to a three dimensional (3D) gel network in which the solvent was incorporated (Figures 1 and 2, when t=0hr). Neither less hydrolysis or over hydrolysis can provide a transparent and immobile 3D gel structure (Scheme 1)

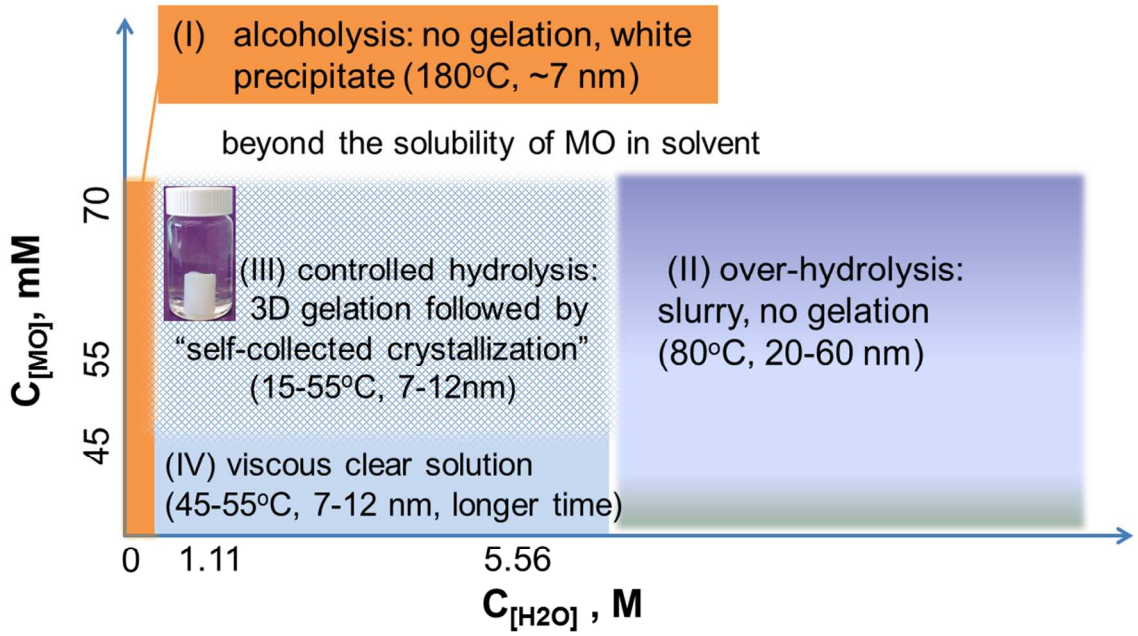

Scheme 1. Relation between the concentrations of water and metal-organic species (MO) and gelation (T=15 ˚C). Note: The x, y axes are not proportional.

Moreover, it was found that a suitable initial BST precursor concentration (e.g. $[Ti(OiPr)_4]$) to form good BST nanocrystal monoliths (or so-called gel rods) in ethanol is in the range of 0.055-0.07 M (Scheme 1, zone III). When the starting concentration of $Ti(OiPr)_4$ is 0.043M or less (Scheme 1, zone IV), a viscous clear solution was formed after 2 days of room temperature (15 ˚C) aging, and the complete crystallization occurred in 11hrs at 55 ˚C or in 20 hrs at 45 ˚C (Figure 6), but it would not occur at 15 ˚C even after a month. Instead of the above monolith, a stable and transparent nanocrystal solution was eventually formed (Figure 6), which consists of extremely high yield (> 99%) of pure and monodisperse BST crystalline phase and ethanol solvent as well as trace amount of isopropanol and water from the crystallization process. In addition, the nanocrystal solution is super stable (~10 mg/ml), which can be used directly for thin film fabrication without further separation and purification. The stable and transparent solution may also be used as a potential smart electro-rheological fluid materials [4]. It is worth mentioning that at a high temperature above 180 ˚C the originally viscous solution may finally form a nanocrystalline monolith because of improved interconnection among nanocrystals. On the other hand, when increasing the initial concentration $[Ti(OiPr)_4]$ to the range of 0.055-0.07 M, the initial clear solution can gradually turn into a viscous solution and finally into an immobile clear

gel within hours, which can be gradually converted to a solid nanocrystal gel monolith (or "gel rod") as well as a separated clear liquid phase through continuous shrinkage of the original gel in the temperature range of 15 ˚C and 55 ˚C (Figure 6).

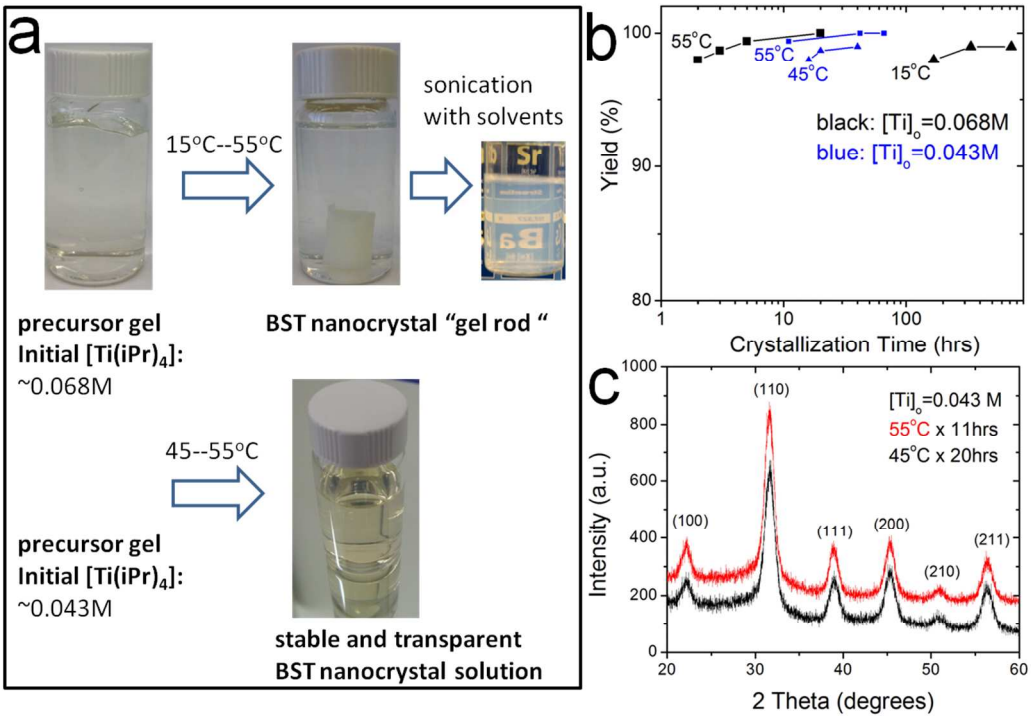

Figure 6. Synthesis of BST nanocrystals and solution as a function of initial metalorganic source concentration, temperature and time. (a) photo images of as-synthesized nanocrystals with different initial concentrations; (b) BST yields as a function of initial concentration and crystallization time, and (c) XRD patterns of BST nanocrystals synthesized at different temperatures under lower initial concentration.

Before heating, a period of aging at room temperature favors A site cations coordinate more homogeneously which follows the B site cations stereo crosslink through the formation of B-O-B bonds (in perovskite ABO_3 structure, A=Ba, Sr; B=Ti, Zr, Hf, etc), an intermediate to final pure and highly crystallized products, and to avoid byproducts due to less controlled hydrolysis. Generally, transparent and immobile gels incorporated with liquid solvent can be formed after the aging process. The following crystallization of products occurs at a low temperature of 15-55 ˚C for as short as hours under static conditions, and the as-synthesized nanocrystals self-accumulate to form crystallized solid gel monoliths over the time, while the liquid phase is gradually expelled out of the network. It results in a well separation of the solid products from the solvent and liquid byproducts (Figures 1 and S5, t=2-6 hrs). The crystallization is a slow process and a rate-determined step. The higher the temperature, the faster the crystallization proceeds and the faster the crystalline "gel rod" forms (Figure 1 and graphic abstract). Many oxides can be synthesized by the present method with forming a crystalline gel rod at low

temperatures. Hence, to understand the detail of the reaction mechanism of the method it is essential for further precisely controlling reaction and expansion of the present method to synthesize more complex oxides (w/o dopants) with different crystal structures at low temperature. A possible growth mechanism is described in Supplementary information, Scheme S1

Previously, it was reported that $BaTiO_3$ nanocrystals were synthesized by a sol-gel process involving the delivery of acidic water vapor at the gas-liquid interface of a bimetallic alkoxide[11]. The process used somewhat toxic methanol/2-methoxyethanol first and later switched to less toxic methoxypropanol/1-butanol mixed solvent to dissolve BST precursors, plus it relies on acidic water vapor (HCl) as a catalyst to induce the hydrolysis and crystallization. However, the complex apparatus required for the kinetically controlled delivery and synthesis as well as the corrosive nature of acidic vapor may be concerns for further large scale production. In our synthesis scheme, simple alcohol such as ethanol was used to replace the high boiling point mixed solvents, and the hydrolysis of metal alkoxides was controlled with trace amount of water in ethanol (2-5 vol%). Once the metal organic sources were dissolved, no further stirring was necessary. The following gelation and crystallization/ product self-collection can occur in a regular container with a closed lid at a low temperature under static conditions with no stirring involved.

The self-collection synthesis may be regarded as a green process compared to other sol-gel processes because (1) it uses less energy. Simple synthesis apparatus (such as regular glass or plastic containers with lids, s-Figure 5) and simplified procedures are applied to synthesize highly crystalline and pure perovskite oxide nanocrystals. Stirring is only needed at the beginning for dissolving metal organic sources to provide a clear solution, and the following gelation, crystallization/ product self-collection all occurred at a low temperature of 15-55^{o}C under static conditions. With controlled amount of water, the nanocrystal product is self-accumulated to form a monolith with extremely high yield so that it can be easily collected and purified without going through energy intensive centrifugation-separation process. Because the nanocrystals have abundant surface hydroxyl groups and are loosely contacted in the monolith, they can be readily functionalized or uniformly dispersed in alcohol solvents and other media using general sonication to provide stable and transparent solution in the absence of surfactants or stabilizers for the purpose of various incorporation and thin film fabrication; (2) it provides nearly 100% yield of pure nanocrystal products with no contamination and less waste. Since metal organic sources can be fully converted to pure and highly crystalline solid products that are self-collected and well separated from a clear liquid phase, almost 100% high yield and selectivity can be achieved for the desired products after separation and purification. On the other hand, besides the ligand-free pure nanocrystal product, the only byproduct is isopropanol, so the liquid phase is recyclable, leaving little waste in the end. It was demonstrated that BST nanocrystals of equally high quality can also be synthesized in co-solvent of isopropanol/ethanol (0-1 by volume).

Because of simple setup, static synthesis condition, simplified procedures from synthesis to separation/purification, and self-collection of products with sizes only sensitive to controlled trace water content, the green process suggests that the production is easy for upscale production while maintaining high crystallinity, phase purity and monodispersity (Supplementary Figs. S7 and S8). For instance, a BST nanocrystal monolith was prepared from corresponding amorphous clear gel at 45^{o}C for 6 hrs in a 250 ml polymer container (polystyrene, or PS). The synthesis was also conducted in other containers made of glass or polyethylene (PE) (s-Figure 8), and the as-collected gel monoliths don't stick on the wall. The as-synthesized nanocrystal gel monoliths were easily collected by removing the liquid phase. After a simple rinsing with ethanol solvent, the nanocrystal products can be readily dispersed in a variety of polar solvents such as ethanol, DMF, and furfural alcohol (FA) using a simple sonication process to afford stable nanocrystal solution. The aggregate free BST nanocrystals show high crystallinity and high purity and have a uniform crystal size of ~7.3 ±0.7 nm in diameter (Supplementary Fig. S9). Moreover, the self-collection strategy has been successfully applied to synthesize other complex metal oxides[15].

Conclusion

We report a simple, scalable and green synthesis process to highly crystalline and pure aggregate-free perovskite oxide nanocrystals (such as BT, BST and BSTH) with uniform and tunable sizes at a low temperature between 15 ˚C and 55 ˚C under static conditions, based on a self-collection strategy of the ligand-free nanocrystals from a clear metal-organic solution containing controlled trace amount of water. The process involves dissolving, aging, gelation and crystallization/product self-collection that does not require complicate external drivers (just static conditions and a bit warming). The concentrations of water and metal-organic sources are well controlled so that the slow hydrolysis, cross-linking of the metal-organic sources and complete crystallization under static conditions result in self-accumulation of all the sources into a crystalline solid gel monolith as well as the formation of a clear liquid phase. Thus, the solid monolith composed of loosely contacted nanocrystals can be easily separated from the liquid phase, which is recyclable. As a result, the green process may achieve almost 100% yield of perovskite oxide nanocrystals with less waste. In addition, the green process can be readily scaled up because of its simplified procedure, self-collection of products with sizes less dependent to stirring and temperature control while making high quality nanocrystals and transparent nanocrystal solution. Moreover, in the absence of surfactant or stabilizer, the ligand-free nanocrystals show good dispersibility in polar solvents due to the surface hydrophilicity and surface charges. The super stable perovskite oxide nanocrystal solution has demonstrated great capability for making high performance dielectric thin films.

Acknowledgements

This work was supported by the Advanced Research Project Agency for Energy (ARPA-e), ADEPT DE-AR0000114, and the National Science Foundation under award NSF IDR #1014777. This work was also partially supported by the Center for Exploitation of Nanostructures in

Sensors and Energy Systems (CENSES) under NSF Cooperative Agreement Award Number 0833180 and South University of Science and Technology of China (SUSTC) . (Talent Development Starting Fund from Shenzhen Government), and Chongqing Funds for Distinguished Young Scientists of cstc2013jcyjjq5001.We are grateful to Prof. Dongyuan Zhao of Fudan University for useful discussions concerning this work. S.O. and W.L are grateful to Prof. Teresa Bandosz for use of the TGA/DTA instrument, and to Karifala Kante for his assistance in recording the data.

Reference

1. (a) Fell, J. N. F.; Livingston, F. E.; Sarney, W. L.; Niesz, K.; Ould-Ely, T.; Tao, A. R.; Morse, D. E.; Swaminathan, V. S., <title>Bio-inspired synthesis and laser processing of nanostructured barium titanate thin films: implications for uncooled IR sensor development</title>. **2009,** *7321*, 73210I-73210I-13; (b) Eerenstein, W.; Mathur, N. D.; Scott, J. F., Multiferroic and magnetoelectric materials. *Nature* **2006,** *442* (7104), 759-765; (c) Kobayashi, Y.; Hernandez, O. J.; Sakaguchi, T.; Yajima, T.; Roisnel, T.; Tsujimoto, Y.; Morita, M.; Noda, Y.; Mogami, Y.; Kitada, A.; Ohkura, M.; Hosokawa, S.; Li, Z.; Hayashi, K.; Kusano, Y.; Kim, J.; Tsuji, N.; Fujiwara, A.; Matsushita, Y.; Yoshimura, K.; Takegoshi, K.; Inoue, M.; Takano, M.; Kageyama, H., An oxyhydride of BaTiO3 exhibiting hydride exchange and electronic conductivity. *Nat Mater* **2012,** *11* (6), 507-11; (d) Kotecki, D. E.; Baniecki, J. D.; Shen, H.; Laibowitz, R. B.; Saenger, K. L.; Lian, J. J.; Shaw, T. M.; Athavale, S. D.; Cabral, C.; Duncombe, P. R.; Gutsche, M.; Kunkel, G.; Park, Y. J.; Wang, Y. Y.; Wise, R., (Ba,Sr)TiO3 dielectrics for future stacked-capacitor DRAM. *Ibm Journal of Research and Development* **1999,** *43* (3), 367-382; (e) Polking, M. J.; Han, M.-G.; Yourdkhani, A.; Petkov, V.; Kisielowski, C. F.; Volkov, V. V.; Zhu, Y.; Caruntu, G.; Paul Alivisatos, A.; Ramesh, R., Ferroelectric order in individual nanometre-scale crystals. *Nature Materials* **2012,** *11* (8), 700-709; (f) Ramesh, R.; Spaldin, N. A., Multiferroics: progress and prospects in thin films. *Nat Mater* **2007,** *6* (1), 21-9; (g) Valencia, S.; Crassous, A.; Bocher, L.; Garcia, V.; Moya, X.; Cherifi, R. O.; Deranlot, C.; Bouzehouane, K.; Fusil, S.; Zobelli, A.; Gloter, A.; Mathur, N. D.; Gaupp, A.; Abrudan, R.; Radu, F.; Barthelemy, A.; Bibes, M., Interface-induced room-temperature multiferroicity in BaTiO(3). *Nat Mater* **2011,** *10* (10), 753-8; (h) Yan, Z.; Guo, Y.; Zhang, G.; Liu, J. M., High-Performance Programmable Memory Devices Based on Co-Doped BaTiO3. *Advanced Materials* **2011,** *23* (11), 1351-1355; (i) Brutchey, R. L.; Cheng, G.; Gu, Q.; Morse, D. E., Positive Temperature Coefficient of Resistivity in Donor-Doped BaTiO3 Ceramics derived from Nanocrystals synthesized at Low Temperature. *Advanced Materials* **2008,** *20* (5), 1029-1033; (j) Huang, L. M.; Jia, Z.; Kymissis, I.; O'Brien, S., High K Capacitors and OFET Gate Dielectrics from Self-Assembled BaTiO3 and (Ba,Sr)TiO3 Nanocrystals in the Superparaelectric Limit. *Adv. Funct. Mater.* **2010,** *20* (4), 554-560.

2. (a) Rabuffetti, F. A.; Lee, J. S.; Brutchey, R. L., Low Temperature Synthesis of Complex Ba1–xSrxTi1–yZryO3Perovskite Nanocrystals. *Chemistry of Materials* **2012,** *24* (16), 3114-3116; (b) Suntivich, J.; May, K. J.; Gasteiger, H. A.; Goodenough, J. B.; Shao-Horn, Y., A Perovskite Oxide Optimized for Oxygen Evolution Catalysis from Molecular Orbital Principles. *Science* **2011,** *334* (6061), 1383-1385; (c) Nuraje, N.; Dang, X.; Qi, J.; Allen, M. A.; Lei, Y.;

Belcher, A. M., Biotemplated Synthesis of Perovskite Nanomaterials for Solar Energy Conversion. *Advanced Materials* **2012,** *24* (21), 2885-2889.
3. Kang, B. J.; Lee, C. K.; Oh, J. H., All-inkjet-printed electrical components and circuit fabrication on a plastic substrate. *Microelectronic Engineering* **2012,** *97*, 251-254.
4. Mimura, K.-i.; Nishimoto, Y.; Orihara, H.; Moriya, M.; Sakamoto, W.; Yogo, T., Synthesis of Transparent and Field-Responsive BaTiO3 Particle/Organosiloxane Hybrid Fluid. *Angewandte Chemie International Edition* **2010,** *49* (29), 4902-4906.
5. Glushchenko, A.; Il Cheon, C.; West, J.; Li, F. H.; Buyuktanir, E.; Reznikov, Y.; Buchnev, A., Ferroelectric particles in liquid crystals: Recent frontiers. *Molecular Crystals and Liquid Crystals* **2006,** *453*, 227-237.
6. (a) Ĉulić-Viskota, J.; Dempsey, W. P.; Fraser, S. E.; Pantazis, P., Surface functionalization of barium titanate SHG nanoprobes for in vivo imaging in zebrafish. *Nature Protocols* **2012,** *7* (9), 1618-1633; (b) Ciofani, G.; Danti, S.; D'Alessandro, D.; Moscato, S.; Petrini, M.; Menciassi, A., Barium Titanate Nanoparticles: Highly Cytocompatible Dispersions in Glycol-chitosan and Doxorubicin Complexes for Cancer Therapy. *Nanoscale Research Letters* **2010,** *5* (7), 1093-1101.
7. (a) Kim, P.; Doss, N. M.; Tillotson, J. P.; Hotchkiss, P. J.; Pan, M.-J.; Marder, S. R.; Li, J.; Calame, J. P.; Perry, J. W., High Energy Density Nanocomposites Based on Surface-Modified BaTiO3 and a Ferroelectric Polymer. *ACS Nano* **2009,** *3* (9), 2581-2592; (b) Dang, Z.-M.; Yuan, J.-K.; Yao, S.-H.; Liao, R.-J., Flexible Nanodielectric Materials with High Permittivity for Power Energy Storage. *Advanced Materials* **2013,** *25* (44), 6334-6365; (c) Hao, Y.; Wang, X.; Li, L., Highly dispersed SrTiO3 nanocubes from a rapid sol-precipitation method. *Nanoscale* **2014,** *6* (14), 7940-7946; (d) Hao, Y.; Wang, X.; Kim, J.; Li, L., Rapid Formation of Nanocrystalline BaTiO3 and Its Highly Stable Sol. *Journal of the American Ceramic Society* **2014,** *97* (11), 3434-3441.
8. (a) Park, K.-I.; Lee, M.; Liu, Y.; Moon, S.; Hwang, G.-T.; Zhu, G.; Kim, J. E.; Kim, S. O.; Kim, D. K.; Wang, Z. L.; Lee, K. J., Flexible Nanocomposite Generator Made of BaTiO3 Nanoparticles and Graphitic Carbons. *Advanced Materials* **2012,** *24* (22), 2999-3004; (b) Park, K.-I.; Xu, S.; Liu, Y.; Hwang, G.-T.; Kang, S.-J. L.; Wang, Z. L.; Lee, K. J., Piezoelectric BaTiO3Thin Film Nanogenerator on Plastic Substrates. *Nano Letters* **2010,** *10* (12), 4939-4943; (c) Kim, P.; Jones, S. C.; Hotchkiss, P. J.; Haddock, J. N.; Kippelen, B.; Marder, S. R.; Perry, J. W., Phosphonic Acid-Modified Barium Titanate Polymer Nanocomposites with High Permittivity and Dielectric Strength. *Advanced Materials* **2007,** *19* (7), 1001-1005.
9. (a) Basile, N.; Gonon, M.; Petit, F.; Cambier, F., Interaction between laser beam and BaTiO3 powders in selective laser sintering treatments. *Journal of the European Ceramic Society* **2012,** *32* (12), 3303-3311; (b) Shimooka, H.; Kohiki, S.; Kobayashi, T.; Kuwabara, M., Preparation of translucent barium titanate ceramics from sol-gel-derived transparent monolithic gels. *Journal of Materials Chemistry* **2000,** *10* (7), 1511-1512.
10. (a) O'Brien, S.; Brus, L.; Murray, C. B., Synthesis of monodisperse nanoparticles of barium titanate: Toward a generalized strategy of oxide nanoparticle synthesis. *Journal of the American Chemical Society* **2001,** *123* (48), 12085-12086; (b) Wang, X.; Zhuang, J.; Peng, Q.; Li, Y., A general strategy for nanocrystal synthesis. *Nature* **2005,** *437* (7055), 121-124; (c) Su, K.; Nuraje, N.; Yang, N.-L., Open-Bench Method for the Preparation of BaTiO3, SrTiO3, and BaxSr1-xTiO3Nanocrystals at 80 °C. *Langmuir* **2007,** *23* (23), 11369-11372; (d) Liu, H.; Hu, C.; Wang, Z. L., Composite-hydroxide-mediated approach for the synthesis of nanostructures of complex functional-oxides. *Nano Letters* **2006,** *6* (7), 1535-1540; (e) Adireddy, S.; Lin, C.; Cao,

B.; Zhou, W.; Caruntu, G., Solution-Based Growth of Monodisperse Cube-Like BaTiO3 Colloidal Nanocrystals. *Chemistry of Materials* **2010,** *22* (6), 1946-1948; (f) Kobayashi, Y.; Kosuge, A.; Konno, M., Fabrication of high concentration barium titanate/polyvinylpyrrolidone nano-composite thin films and their dielectric properties. *Applied Surface Science* **2008,** *255* (5, Part 2), 2723-2729; (g) Nuraje, N.; Su, K.; Haboosheh, A.; Samson, J.; Manning, E. P.; Yang, N. L.; Matsui, H., Room temperature synthesis of ferroelectric barium titanate nanoparticles using peptide nanorings as templates. *Advanced Materials* **2006,** *18* (6), 807-+.

11. (a) Ould-Ely, T.; Luger, M.; Kaplan-Reinig, L.; Niesz, K.; Doherty, M.; Morse, D. E., Large-scale engineered synthesis of BaTiO3 nanoparticles using low-temperature bioinspired principles. *Nature Protocols* **2011,** *6* (1), 97-104; (b) Rabuffetti, F. A.; Brutchey, R. L., Structural evolution of BaTiO(3) nanocrystals synthesized at room temperature. *J Am Chem Soc* **2012,** *134* (22), 9475-87; (c) Kobayashi, T.; Matsuda, H.; Kuwabara, M., Shift of Optical Absorption Edge in Sol-Gel Derived Transparent BaTiO3 Gels During Aging. *Journal of Sol-Gel Science and Technology* **1999,** *16* (1-2), 165-171.

12. Tao, A. R.; Habas, S.; Yang, P., Shape Control of Colloidal Metal Nanocrystals. *Small* **2008,** *4* (3), 310-325.

13. (a) Zhou, T.; Zha, J. W.; Cui, R. Y.; Fan, B. H.; Yuan, J. K.; Dang, Z. M., Improving dielectric properties of BaTiO(3)/ferroelectric polymer composites by employing surface hydroxylated BaTiO(3) nanoparticles. *ACS Appl Mater Interfaces* **2011,** *3* (7), 2184-8; (b) Almadhoun, M. N.; Bhansali, U. S.; Alshareef, H. N., Nanocomposites of ferroelectric polymers with surface-hydroxylated BaTiO3 nanoparticles for energy storage applications. *Journal of Materials Chemistry* **2012,** *22* (22), 11196.

14. Huang, L. M.; Liu, S. Y.; Van Tassell, B. J.; Liu, X. H.; Byro, A.; Zhang, H. N.; Leland, E. S.; Akins, D. L.; Steingart, D. A.; Li, J.; O'Brien, S., Structure and performance of dielectric films based on self-assembled nanocrystals with a high dielectric constant. *Nanotechnology* **2013,** *24* (41).

15. Liu, S. Y.; Akbashev, A. R.; Yang, X. H.; Liu, X. H.; Li, W. L.; Zhao, L.; Li, X.; Couzis, A.; Han, M. G.; Zhu, Y. M.; Krusin-Elbaum, L.; Li, J.; Huang, L. M.; Billinge, S. J. L.; Spanier, J. E.; O'Brien, S., Hollandites as a new class of multiferroics. *Scientific Reports* **2014,** *4*, 6.

Graphic abstract

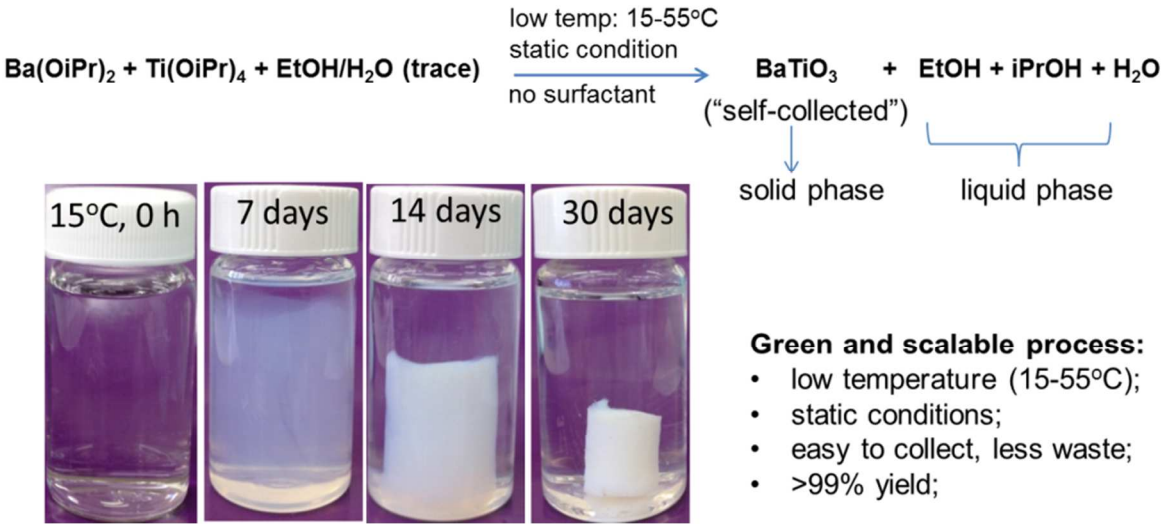

Green scalable "self-collection" growth method to produce uniform and aggregate-free colloidal perovskite oxide nanocrystals in presence of surfactant was reported.